NANO LETTERS
2004
Vol. 4, No. 8
1507−1511

Sub-100 nm Triangular Nanopores Fabricated with the Reactive Ion Etching Variant of Nanosphere Lithography and Angle-Resolved Nanosphere Lithography

Alyson V. Whitney,[†] Benjamin D. Myers,[‡] and Richard P. Van Duyne*[,†]

Department of Chemistry, Northwestern University, 2145 Sheridan Road, Evanston, Illinois 60208-3113, and Department of Materials Science and Engineering, Northwestern University, 2220 Campus Drive, Evanston, Illinois 60208

Received May 3, 2004; Revised Manuscript Received June 8, 2004

ABSTRACT

Nanosphere lithography (NSL) is combined with reactive ion etching (RIE) to fabricate ordered arrays of in-plane, triangular cross-section nanopores. Nanopores with in-plane widths ranging from 44 to 404 nm and depths ranging from 25 to 250 nm are demonstrated. The combination of angle-resolved nanosphere lithography (AR NSL) and RIE yields an additional three-fold reduction in nanopore size.

Arrays of nanoparticles and nanopores in the sub-100 nm size regime are widely used in applications such as catalysis,[1,2] sensing,[3−5] optics,[6] molecular separation,[7−10] molecular reaction dynamics,[11] single-molecule detection,[12] and electronics.[13] Consequently, there is an increasing demand for rapid, massively parallel fabrication strategies for these nanostructures. The standard lithographic techniques used to fabricate such nanostructures with controlled size, shape, and spacing include photolithography, electron beam lithography (EBL),[14] and focused ion beam lithography (FIB).[7] Photolithography is the most widely used because it is massively parallel; however, its resolution is often limited by diffraction to ~100 nm.[15] Recent work has demonstrated that by modifying traditional photolithographic techniques, sub-50 nm structures can be fabricated.[16] EBL and FIB are capable of producing arbitrary shaped nanoparticles and nanopores with excellent minimum feature size that are ideal for many electronic, optical, and magnetic applications. However, the high cost and serial nature of EBL and FIB present serious challenges to their high volume manufacture. Consequently, much recent research has been focused on the development of alternative parallel lithographic methods. The remainder of this paper will concentrate on the topic of low cost, parallel fabrication of nanopores.

Several parallel lithographic methods have been successfully developed to fabricate nanopores.[5,7,17] Pantano and Walt have chemically etched nanopores onto the distal face of an optical imaging fiber.[5] Because each nanopore is connected to its own optical channel, it may be individually addressed or utilized as part of the entire imaging fiber array.[5] In this technique, the nanopore size is controlled by the dimensions of the imaging fiber's distal tip, resulting in a minimum nanopore diameter of 250 nm. Nanoporous alumina membranes with sub-100 nm pore dimensions have been fabricated by electrochemical anodization.[17] This fabrication method is, however, highly substrate specific. The ideal nanopore fabrication technique would not only be low cost and parallel but would also be substrate independent. The work presented herein demonstrates that the reactive ion etching (RIE) variant of nanosphere lithography (NSL) and angle-resolved nanosphere lithography (AR NSL) is a novel nanofabrication approach that yields sub-100 nm nanopores and possesses these desirable properties.

NSL has been shown to be a low cost, parallel, substrate independent technique for producing well-ordered sub-100 nm array structures with nanometer precision.[18] It is based on the self-assembly of polystyrene or silica nanospheres into close-packed monolayers or bilayers, which are then employed as lithographic masks to fabricate nanoparticle arrays. As in all naturally occurring crystals, NSL masks include a variety of defects that arise as a result of nanosphere polydispersity, site randomness, point defects (vacancies), line defects (slip dislocations), and polycrystalline domains.[19] Typical defect-free domain sizes are in the 10−100 μm^2 range.[19] Single layer NSL masks yield nanostructures with a triangular in-plane shape and P_6mm array symmetry. Usually the sample is mounted in a physical vapor deposition

* Corresponding author. E-mail: vanduyne@chem.northwestern.edu.
† Department of Chemistry.
‡ Department of Materials Science and Engineering and NUANCE Center.

10.1021/nl049345w CCC: $27.50 © 2004 American Chemical Society
Published on Web 06/30/2004

system where a material is deposited normal to the substrate surface.[18] The size and interparticle spacing of the resulting nanoparticles are controlled completely by the diameter of the chosen nanospheres. This technique is, therefore, substrate independent. The in-plane width, a, of the nanoparticles produced with a single layer nanosphere mask can be predicted with eq 1.[19]

$$a = \frac{3}{2}\left(\sqrt{3} - 1 - \frac{1}{\sqrt{3}}\right)D \tag{1}$$

AR NSL provides additional control of the size and shape of nanoparticles. The dimensions of AR NSL fabricated nanoparticles are controlled with two additional parameters: (1) the angle between the surface normal of the NSL substrate and the propagation vector of the material deposition beam (Θ) and (2) the azimuthal angle (Φ).[20] Both Θ and Φ can be varied to produce a variety of nanoparticle geometries and interparticle spacing. Furthermore, the size and shape of the fabricated nanoparticles can be accurately predicted using the geometric model developed in our previous work.[20,21]

In this paper, we demonstrate that the combination of NSL and AR NSL with RIE is capable of fabricating size-tunable triangular nanopores in single crystal silicon (111) (Si (111)) substrates. RIE is a natural choice to use with NSL masks because of its parallel and highly anisotropic properties. Because of its anisotropic nature, RIE can also be combined with AR NSL to further reduce the nanopore dimensions. Specifically, it will be shown that this combination approach is ideal for the creation of nanopores with the following unique properties: (1) extremely uniform nanopores (in-plane widths = 44 nm − 404 nm); (2) controlled nanopore depth (25 nm−250 nm); (3) controlled, uniform nanopore shapes; and (4) high areal density ($\sim 10^{10}$ pores cm^{-2}). The in-plane widths of the nanopores are shown to be linearly dependent upon nanosphere diameter, allowing for the production of predetermined, size-tunable nanopores. AR NSL is employed to achieve a three-fold reduction of the nanopore dimensions. For example, nanopores fabricated with 720 nm diameter NSL etch-masks were found to have an average in-plane width of 297 nm. Combining AR NSL and RIE with the same diameter NSL etch-masks produced nanopores with in-plane widths of 93−177 nm. By extrapolation, it is reasonable to suggest that nanopores with in-plane widths of 44 nm can be reduced to ~15 nm using RIE and AR NSL.

Phosphorus doped Si (111) substrates were purchased from Wacker Siltronic (Portland, OR) and cut into ~10 mm^2−15 mm^2 pieces. The substrates were cleaned in a piranha etch solution (30% 3:1 H_2SO_4/H_2O_2) for 30 min at 80 °C in order to create a hydrophilic surface on Si (111) to facilitate self-assembly of the nanosphere masks. After rinsing with water, the silicon substrates were sonicated for 60 min in 5:1:1 H_2O/H_2O_2/NH_4OH. Finally, the silicon substrates were rinsed and stored in water for future use.

Surfactant-free carboxyl-terminated polystyrene nanospheres of specific diameters (1100−160 nm) were self-assembled on to the Si (111) substrates as described in previous work.[22] The sample was then placed in an RIE chamber (RIE 2000, South Bay Technology) and etched with a CF_4 plasma. Unless otherwise stated, etch conditions were as follows: etch time = 2 min, radio frequency power = 45 W, chamber pressure = 20 mTorr, DC−bias = −500 − −600 V, and flow rate = 72 sccm. When the reactive plasma bombards the polystyrene nanospheres, the hydrocarbons are fluorinated and remain intact. However, interaction between the reactive CF_4 plasma and the Si (111) substrate produces volatile SiF_4, thus etching the exposed surface area. The resulting nanostructure is a well-ordered periodic array of triangular cross-section nanopores. Using this protocol, nanopores with varying in-plane widths were fabricated using nanosphere diameters of 160 nm, 290 nm 510, 720, and 1100 nm.

The fabrication of nanopores by AR NSL and RIE begins with the self-assembled NSL etch mask described above. The sample substrate and etch mask are then mounted on a machined aluminum block in order to obtain the desired angle, Θ. The sample is then placed in the RIE chamber and etched as described above. The geometry of the nanopores was predicted using the symbolic mathematics program Maple 8 (Version 9.0, Waterloo Maple Inc., Ontario, Canada).[20] The Maple worksheet was used to determine the projection of the nanosphere mask onto a substrate for a specified Θ and azimuthal angle Φ. The generated graphical representations of the nanopore shapes were compared to the fabricated nanopore geometries observed with scanning electron microscopy (SEM) (Gemini 1525, Leo). While Θ can be easily controlled by etching geometry, imperfections in the nanosphere mask make it difficult to control Φ, resulting in a single sample containing several nanopore geometries. Determining Φ was done by choosing a value that gave the best overall shape fit for the experimentally controlled Θ values.

Characterization of the nanopore depths and in-plane widths was carried out using tapping mode atomic force microscopy (AFM) (Nanoscope IV microscope and Nanoscope IIIa controller, Digital Instruments). Accurate AFM measurements of nanopore depth are problematic due to the large size of the AFM tip relative to the nanopore aperture. Therefore, to obtain accurate depths, line scans were measured over small defect areas on the substrate surface. In addition, the nanopore depth was measured by further cross-sectional SEM analysis. The etched Si (111) sample was first milled with FIB (FIB-2000A, Hitachi) and then cleaved to obtain a clean edge for SEM examination.

This work demonstrates that nanopore size and shape tunability can be achieved by combining NSL etch masks with RIE. Figure 1 shows AFM images of nanopores in Si (111) fabricated using 290 nm diameter nanospheres as the etch mask along with a corresponding typical line scan. This image contains a small defect area so that the nanopore depth can be accurately determined. A two minute etch with the CF_4 plasma produced nanopores of uniform depth with an average value of 28.3 ± 0.6 nm. Etching times of 2−10 min produced nanopore depths ranging from ~25−250 nm. We

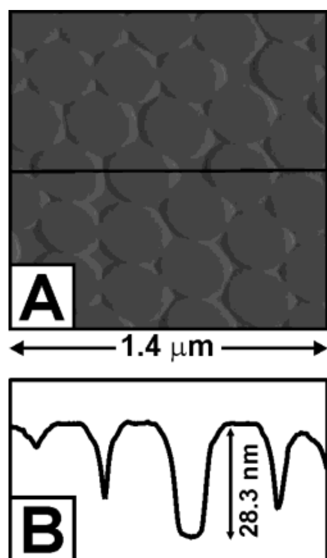

Figure 1. (A) AFM image of nanopores fabricated with a 290 nm nanosphere diameter etch mask on P-doped Si (111) with a typical line scan (B) over a small defect area. Etch time = 2 min and height = 28.3 ± 0.5 nm.

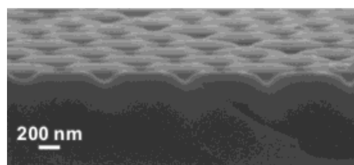

Figure 2. SEM image of a cross-section of nanopores fabricated with a 720 nm diameter nanosphere etch mask with an etch time of 4 min.

anticipate that nanopores with depths in the 1−5 μm range could be produced by using deep reactive ion etching (DRIE) conditions.[23]

A cross-sectional SEM image of an array of typical nanopores is shown in Figure 2. An etch mask assembled from 720 nm diameter nanospheres was used with an etch time of 4 min. AFM line scan analysis determined the average nanopore depth to be 106.0 nm. The cross-sectional SEM image supports this depth measurement. Interestingly, one can see that the nanopores have a tapered shape, which can be attributed to the fact that RIE is not a perfectly anisotropic process.

Nanopore in-plane widths were experimentally determined using AFM line scans and theoretically predicted using eq 1. Figure 3 depicts AFM images of nanopores fabricated with nanosphere etch masks with nanosphere diameters of 720, 290, and 160 nm and corresponding line scans. The in-plane widths of the respective nanopores were experimentally found to be 297.9 ± 13.9 nm, 102.7 ± 6.4 nm, and 44.9 ± 8.4 nm. The propagation vector of the RIE plasma was normal to the Si (111)/nanosphere surface. While the reader may interpret Figure 3 to depict nanoparticles instead of nanopores, the corresponding line scans clearly indicate that they are nanopores. Predicted in-plane widths were calculated from eq 1 for the nanopores shown in Figure 3 and were found to be 167, 67, and 37 nm, corresponding to nanosphere etch masks with diameters of 720, 290, and 160 nm, respectively.

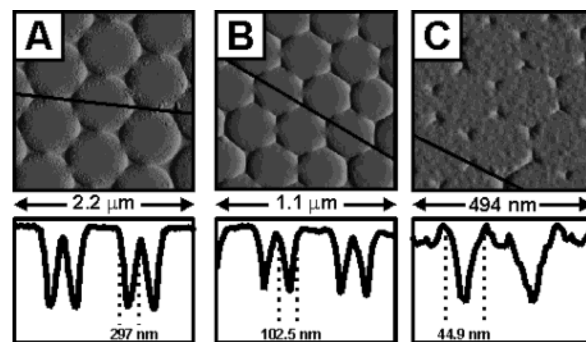

Figure 3. AFM images of several sizes of nanopore structures on Si (111) with corresponding line scans. (A) Nanopores fabricated with 720 nm diameter nanosphere etch mask. In-plane width = 297.9 ± 13.9 nm. (B) Nanopores fabricated with 290 nm diameter nanosphere etch mask. In-plane width = 102.5 ± 6.4 nm. (C) Nanopores fabricated with 160 nm diameter nanosphere etch mask. In-plane width = 44.9 ± 3.8 nm. (C) Etch time = 1 min, RF power = 26 W.

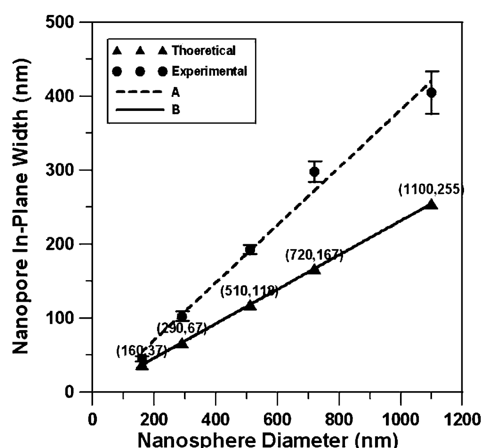

Figure 4. Plot of both experimental and theoretical nanopore in-plane widths with relation to nanosphere etch mask diameters. (A) $Y = 0.4X - 7.8$, $R^2 = 0.9883$, (B) Plot of eq 1: $a = (3/2)(\sqrt{3} - 1 - (1/\sqrt{3})D$ with coordinates that correspond to experimental data.

Figure 4 is a plot of experimental and predicted (from eq 1) nanopore in-plane widths as a function of nanosphere diameter. The experimental in-plane widths are always found to be greater than those predicted from eq 1. This discrepancy can be attributed to three factors. The first factor is the convolution of the AFM tip radius of curvature with the nanopore, resulting in systematic errors in the measured in-plane widths.[24] The experimental values have a y-intercept of −7.84 nm. This deviation is also a consequence of AFM tip convolution. The second factor is that since the nanospheres contain only one point of direct contact with the substrate, the etchant can access the substrate underneath the nanosphere mask (underetching). The third factor is that the etching species may scatter off the NSL mask and in doing so create nanopore apertures that are larger than would otherwise be predicted. While the theoretical model does not quantitatively predict the nanopore in-plane widths, the fabricated nanopore dimensions were a linear function of nanosphere diameter, therefore the fabricated nanopore in-

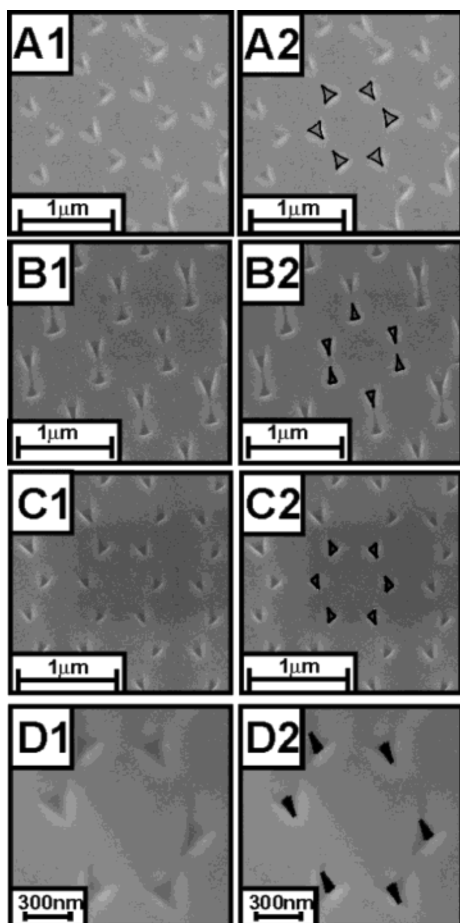

Figure 5. SEM images of nanopores fabricated using AR NSL and images with simulated superimposed geometries, respectively. (A1, A2) $\Theta = 20°$, $\Phi = 5°$; (B1, B2) $\Theta = 30°$, $\Phi = 1°$; (C1, C2) $\Theta = 30°$, $\Phi = 24°$; and (D1, D2) $\Theta = 40°$, $\Phi = 10°$. All nanopores were made with 720 nm nanosphere etch masks on Si (111). Etch time = 2 min.

plane widths can be designed to a predetermined size. The slope of the experimental values is a factor of 2 larger than the slope of the theoretical values. The origin of the factor of 2 slope difference is due to underetching as well as scattering of the etching species. The etchant has more access to etch underneath large nanospheres than small nanospheres. Furthermore, the larger nanospheres provide a wider angular distribution for the scattered etching species, resulting in larger nanopore apertures.

The RIE variant of AR NSL yields a further reduction in nanopore in-plane widths by approximately a factor of 3. Furthermore, a variety of nanopore aperture shapes are possible with AR NSL. Figure 5 depicts SEM images of the resulting nanopores (5A-1, 5B-1, 5C-1, and 5D-1) paired with their theoretically predicted geometric representations (5A-2, 5B-2, 5C-2, and 5D-2). All nanopore structures shown in Figure 5 were designed with 720 nm diameter etch masks. A range of Θ (20°−40°) and Φ (1°−24°) values were used in the modeling. One can see how drastically the angle Φ affects the final nanopore dimensions. Figures 5B and 5C show nanopores that have both been etched at $\Theta = 30°$ while their Φ values vary dramatically. The resulting pore aperture shapes are significantly different. The in-plane widths ranged from 93 to 177 nm, demonstrating a three-fold decrease in the dimensions of the nanopore aperture. The geometrically predicted representations of the pore apertures corresponded well with small values of Θ ($\leq$30°) seen in the SEM images (Figures 5A-2, 5B-2, and 5C-2). However, as seen in Figure 5D-2, at larger values of Θ the predicted geometric representations fail to match well with the experimental results. The nanopores fabricated at $\Theta = 40°$ were significantly larger than the predicted geometry. This deviation can be attributed to the fact that at large values of Θ, significant underetching of the nanosphere mask occurs. One can expect that as Θ increases, the fabricated nanopores will deviate further from their predicted geometry because of underetching. Furthermore, tilting of the substrate will affect the uniformity of the etching parameters, which would become more significant as Θ increases, resulting in further deviation of the experimental nanopore geometry from the predicted nanopore geometry.

In conclusion, we have shown that the RIE variant of NSL and AR NSL can be employed to make sub-100 nm triangular nanopores which have potential applications in catalysis, optics, magnetics, sensing, molecular separation, molecular dynamics, and single-molecule detection. The nanopores presented here have the following unique characteristics: (1) uniform in-plane-widths (44−404 nm), (2) controlled depth (25−250 nm), (3) controlled shapes, and (4) high areal density ($\sim 10^{10}$ pores cm^{-2}). Furthermore, we have shown that AR NSL provides an additional three-fold reduction in the in-plane width of the nanopores. Because the in-plane width has been shown to be linearly dependent on nanosphere diameter, the fabrication of predetermined, size-tunable nanopores is possible. AR NSL provides additional control of nanopore dimension by utilizing the parameters Θ and Φ. This technique was employed to etch nanopores through 720 nm diameter nanosphere etch masks with in-plane widths ranging from 93 to 177 nm, resulting in a three-fold reduction in nanopore dimensions compared to those fabricated with $\Theta = 0°$. The nanopore geometries fabricated with AR NSL and RIE corresponded well with the theoretically determined geometries for values of $\Theta \leq$ 30°. Because of their size uniformity, these nanopores provide the ideal template to fabricate a variety of optical and magnetic nanoparticles. Future work will focus on extending this nanopore fabrication technique to a variety of substrates for applications in nanoparticle optics, nanomagnetics, and catalysis.

Acknowledgment. This work was supported by the Chemical Sciences, Geosciences and Biosciences Division, Office of Basic Energy Sciences, Office of Science, U. S. Department of Energy (DE-FG02-03ER15457) at the Northwestern University Institute for Environmental Catalysis and the Air Force Office of Scientific Research MURI program (F49620-03-1-0381). We are also grateful to the NUANCE facility at Northwestern University for the use of their SEM and FIB.

References

(1) Grunes, J.; Zhu, J.; Anderson, E. A.; Somorjai, G. A. *J. Phys. Chem. B* **2002**, *106*, 11463−11468.
(2) Bronstein, L. M. *Top. Curr. Chem.* **2003**, *226*, 55−89.
(3) Haes, A. J.; Zou, S.; Schatz, G. C.; Van Duyne, R. P. *J. Phys. Chem. B* **2004**, *108*, 109−116.
(4) Riboh, J. C.; Haes, A. J.; McFarland, A. D.; Yonzon, C. R.; Van Duyne, R. P. *J. Phys. Chem. B* **2003**, *107*, 1772−1780.
(5) Pantano, P.; Walt, D. R. *Chem. Mater.* **1996**, *8*, 2832−2835.
(6) Haynes, C. L.; Van Duyne, R. P. *J. Phys. Chem. B* **2003**, *107*, 7426−7433.
(7) Tong, H. D.; Jansen, H. V.; Gadgil, V. J.; Bostan, C. G.; Berenschot, E.; van Rijn, C. J. M.; Elwenspoek, M. *Nano Lett.* **2004**, *4*, 283−287.
(8) Han, J.; Craighead, H. G. *Science* **2000**, *288*, 1026−1029.
(9) Siwy, Z.; Fulinski, A. *Phys. Rev. Lett.* **2002**, *89*, 198103/198101−198103/198104.
(10) Lee, S. B.; Martin, C. R. *Anal. Chem.* **2001**, *73*, 768−775.
(11) Gasparac, R.; Mitchell, D. T.; Martin, C. R. *Electrochim. Acta* **2004**, *49*, 847−850.
(12) Howorka, S.; Cheley, S.; Bayley, H. *Nature Biotechnol.* **2001**, *19*, 636−639.
(13) Landskron, K.; Hatton, B. D.; Perovic, D. D.; Ozin, G. A. *Science* **2003**, *302*, 266−269.
(14) Haynes, C. L.; McFarland, A. D.; Zhao, L. L.; Van Duyne, R. P.; Schatz, G. C.; Gunnarsson, L.; Prikulis, J.; Kasemo, B.; Kall, M. *J. Phys. Chem. B* **2003**, *107*, 7337−7342.
(15) Martin, O. J. F. *Microelectron. Eng.* **2003**, *67*−*68*, 24−30.
(16) Lin, B. J, Labes, K., Eds. *Journal of Microlithography, Microfabrication, and Microsystems* **2004**, *3*, 6−193.
(17) Hulteen, J. C.; Martin, C. R. *J. Mater. Chem.* **1997**, *7*, 1075−1087.
(18) Hulteen, J. C.; Van Duyne, R. P. *J. Vac. Sci. Technol. A* **1995**, *13*, 1553−1558.
(19) Haynes, C. L.; Van Duyne, R. P. *J. Phys. Chem. B* **2001**, *105*, 5599−5611.
(20) Haynes, C. L.; McFarland, A. D.; Smith, M. T.; Hulteen, J. C.; Van Duyne, R. P. *J. Phys. Chem. B* **2002**, *106*, 1898−1902.
(21) Haynes, C. L.; Van Duyne, R. P. *Nano Lett.* **2003**, *3*, 939−943.
(22) Jenson, T. R.; Duval, M. L.; Kelly, K. L.; Lazarides, A. A.; Schatz, G. C.; Van Duyne, R. P. *J. Phys. Chem. B* **1999**, *103*, 9846−9853.
(23) Madou, M. J. *Fundamentals of Microfabrication The Science of Miniaturization*, 2nd ed.; CRC Press: Boca Raton, FL, 2002.
(24) Hulteen, J. C.; Treichel, D. A.; Smith, M. T.; Duval, M. L.; Jenson, T. R.; Van Duyne, R. P. *J. Phys. Chem. B* **1999**, *103*, 3854−3863.

NL049345W